Supporting information: Evaluating random search strategies in three mammals from distinct feeding guilds

Marie Auger-Méthé, Andrew E. Derocher, Craig A. DeMars,

Michael J. Plank, Edward A. Codling, Mark A. Lewis

S1 Variation in threshold angle

In the main text, we used a threshold angle of 10° to estimate biological relevant steps out of the sampled steps. In this Appendix, we show that the results remain largely unchanged when other threshold angles are used. As mentioned in the main text we use the local turn definition to identify important turning events (Reynolds *et al.*, 2007; Codling & Plank, 2011). This method creates a step by amalgamating any consecutive sampled steps that have a turn angle in any direction smaller than the threshold angle (Fig. S1.1). As described in Auger-Méthé *et al.* (2015), we start a new step when: 1) a turn angle, as defined by the sampling time interval, is greater or equal to the threshold angle, 2) at the end of a period of immobility (i.e., the last of a set of consecutive locations that have exactly the same coordinates), and 3) after a missing location. Because missing locations could potentially impact the analyses, we restrained our analyses to movement paths that had $< 30\%$ of the location missing. Fig. S1.2 demonstrates the impact of variation in threshold angle and missing locations on a movement path.

To look at the impact of the threshold angle on the results, we have reapplied the models to our data using threshold angles ranging from $0 - 60°$. Using a threshold angle of 60° includes as forward movement a third of a circle. We constrained the analysis to movement path with at least 50 steps and with $< 30\%$ of the location missing for all threshold angles investigated. This ensured that the analyses with different threshold angles included the same individuals and thus were comparable. Because movement paths defined using high threshold angles have fewer steps, this constraint resulted in a reduced data set compared to the one presented in the main text.

Increasing the threshold angle decreased the number of paths that have one of the CCRWs as their best model and increased the number of paths that have the BW and the TLW as best model (Table S1.1). The mean Akaike weight for CCRWs remained high across threshold angles, with 0.91 as the lowest recorded mean weight (Table S1.1). Regardless of the threshold angle used, some movement paths were not statistically different from the CCRWs. The BW was only selected as best model for caribou movement paths and reached a maximum of seven selected paths when the largest threshold angle (60°) was used. The mean Akaike weight for the BW ranged from 0.39 to 0.63 and many caribou movement paths were not statistically different from the BW. The TLW was only selected as best model for grizzly bear movement paths and reached a maximum of three selected paths when a threshold angle of 40° or 60° was used. The mean Akaike weight of the TLW ranged from 0.90 to 0.93. However, we only found evidence for one movement path that was best described by the TLW and not statistically different from the TLW when the threshold angle of 50° was used (Table S1.1). As for the results presented in the main text, when only the TLW and BW were considered as alternatives there was substantial relative support for the TLW (Table S1.2). Such support increased with increasing the threshold angle. However, there was still only one movement path that was not statistically different from the TLW and only when high threshold angles were used ($50 - 60°$).

Table S1.1: Relative and absolute fit of models when different threshold angles, θ_T, are used. For each model, we present the number of movement paths selected as best model with AIC_c, their mean Akaike weight, and how many of the selected paths are not statistically different from this model when only the step lengths are considered. Our dataset included the movement paths of 22 caribou, 20 grizzly bears, and 11 polar bears.

θ_T (°)	Model	N° as best model			w of best model			N° p-value > 0.05		
		Caribou	Grizzly	Polar bear	Caribou	Grizzly	Polar bear	Caribou	Grizzly	Polar bear
0	$CCRW_A$	6	13	10	0.97	1.00	1.00	2	3	0
	$CCRW_L$	14	7	1				9	4	0
	TLW	0	0	0	–	–	–	–	–	–
	BW	2	0	0	0.39	–	–	0	–	–
	CRW	0	0	0	–	–	–	–	–	–
10	$CCRW_A$	4	15	9	0.95	1.00	1.00	1	1	0
	$CCRW_L$	17	5	2				9	4	0
	TLW	0	0	0	–	–	–	–	–	–
	BW	1	0	0	0.42	–	–	0	–	–
	CRW	0	0	0	–	–	–	–	–	–
20	$CCRW_A$	4	14	9	0.94	0.99	1.00	2	2	0
	$CCRW_L$	17	6	2				11	4	0
	TLW	0	0	0	–	–	–	–	–	–
	BW	1	0	0	0.54	–	–	0	–	–
	CRW	0	0	0	–	–	–	–	–	–
30	$CCRW_A$	4	13	8	0.93	1.00	1.00	0	3	0
	$CCRW_L$	17	5	3				12	2	1
	TLW	0	2	0	–	0.90	–	–	0	–
	BW	1	0	0	0.61	–	–	0	–	–
	CRW	0	0	0	–	–	–	–	–	–
40	$CCRW_A$	4	12	8	0.93	1.00	1.00	2	7	0
	$CCRW_L$	17	5	3				7	3	1
	TLW	0	3	0	–	0.90	–	–	0	–
	BW	1	0	0	0.63	–	–	1	–	–
	CRW	0	0	0	–	–	–	–	–	–
50	$CCRW_A$	4	14	10	0.91	0.98	1.00	3	7	0
	$CCRW_L$	14	4	1				9	1	0
	TLW	0	2	0	–	0.93	–	–	1	–
	BW	4	0	0	0.55	–	–	3	–	–
	CRW	0	0	0	–	–	–	–	–	–
60	$CCRW_A$	5	12	8	0.95	0.97	0.98	2	6	0
	$CCRW_L$	10	5	3				6	4	1
	TLW	0	3	0	–	0.92	–	–	0	–
	BW	7	0	0	0.55	–	–	5	–	–
	CRW	0	0	0	–	–	–	–	–	–

Table S1.2: Relative and absolute fit of the two models generally used in Lévy walk analysis when different threshold angles, θ_{T}, are used to define biologically relevant steps. For each model, we present the number of movement paths selected as best model with AIC_c and the mean Akaike weight of these selected paths. We also present how many of the overall paths are not statistically different from the TLW and BW when only the step lengths are considered. Our dataset included the movement paths of 22 caribou, 20 grizzly bears, and 11 polar bears.

θ_{T} (°)	Model	N° as best model			w of best model			N° p-value > 0.05		
		Caribou	Grizzly	Polar bear	Caribou	Grizzly	Polar bear	Caribou	Grizzly	Polar bear
0	TLW	0	17	1	–	0.99	1.00	0	0	0
	BW	22	3	10	1.00	1.00	1.00	13	1	0
10	TLW	0	15	1	–	1.00	1.00	0	0	0
	BW	22	5	10	1.00	0.93	1.00	11	1	0
20	TLW	0	18	2	–	1.00	0.77	0	0	0
	BW	22	2	9	1.00	0.97	1.00	10	1	0
30	TLW	0	17	2	–	0.99	1.00	0	0	0
	BW	22	3	9	1.00	0.97	1.00	9	0	0
40	TLW	0	18	2	–	1.00	1.00	0	0	0
	BW	22	2	9	1.00	0.86	1.00	12	1	0
50	TLW	0	18	2	–	1.00	1.00	0	1	0
	BW	22	2	9	1.00	0.77	1.00	13	2	0
60	TLW	0	19	3	–	0.98	1.00	0	1	0
	BW	22	1	8	1.00	1.00	1.00	14	1	0

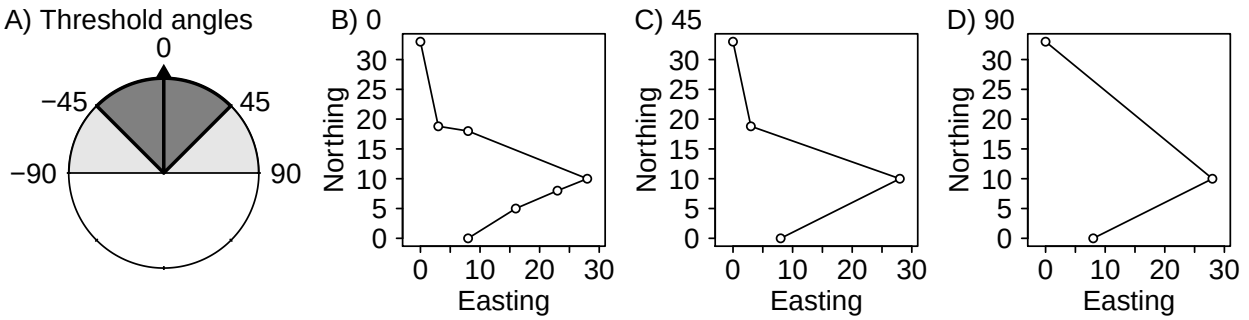

Figure S1.1: Transforming steps defined by regular time intervals into steps defined by the local turn method. (A) Representation of three different threshold angles. The arrow depicts the direction of the previous step. (B) Movement path with five steps as defined by regular time intervals, which correspond to a threshold angle of 0°. (C-D) The same movement path when defined by local turns with a threshold angle of 45 and 90°.

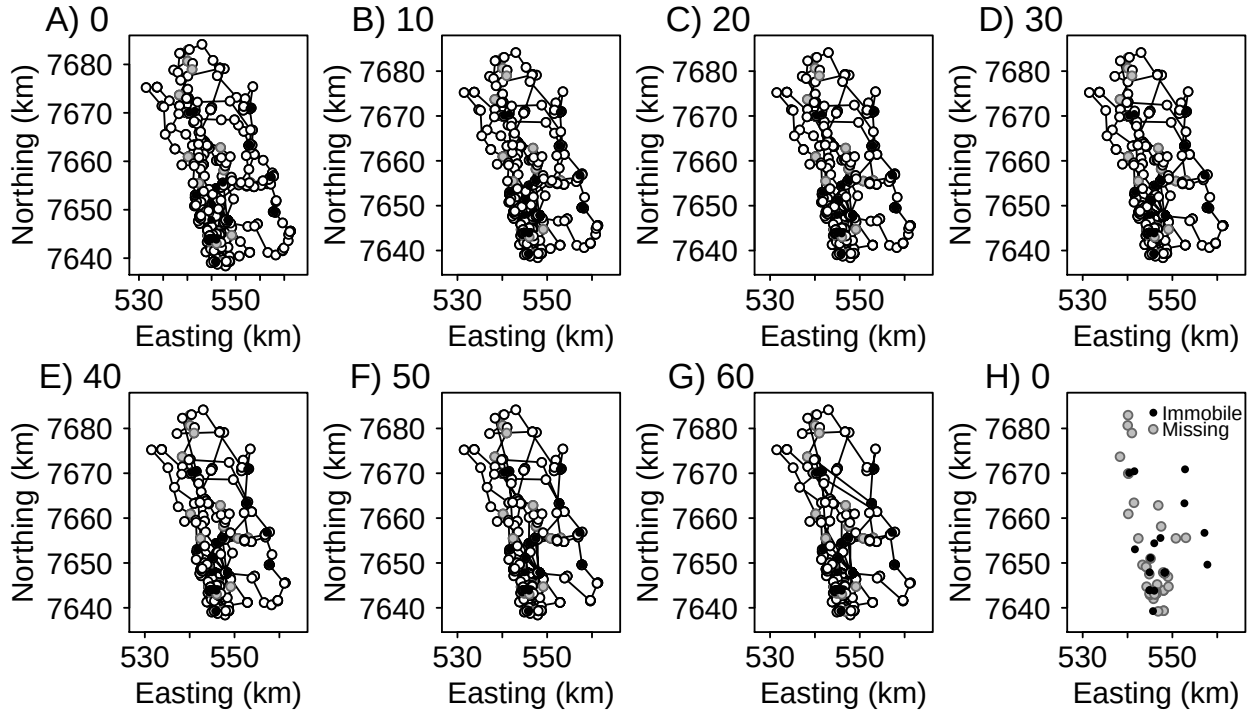

Figure S1.2: Movement path of one grizzly bear for the threshold angles of: (A) 0°, which is the equivalent to using the sampled steps, (B-H) 10-60°, as indicated in the figure. (G) Locations assigned as immobile and for missing, the last location before a missing location is represented. This is the only individual for which an increase in the threshold angle consistently resulted in stronger relative support of the TLW over CCRWs. The best model according to AIC_c is the CCRW_A for threshold angles 0-20° and TLW for threshold angles 30-60°.

S2 Model fit for each individual

In the main text, we present summary values for the model fit results. In this appendix, we present the results from each individual. The results for caribou are found in Table S2.1 and Fig. S2.1, those for grizzly bears are found in Table S2.2 and Fig. S2.2, and those for polar bears are found in Table S2.3 and Fig. S2.3. As the sample size is likely to impact the rejection rate of the test of absolute fit, we present the relationship between the sample size and p-value in Fig. S2.4.

Table S2.1: Delta AICc results for each individual caribou, where n represents the number of steps in the movement path analyzed (using threshold angle of 10°) and '% missing' is the percentage of locations that were missing in the original movement path. We also present the p-value of the test of absolute fit (based on step length distribution) of the best model.

ID	n	% missing	$CCRW_A$	$CCRW_L$	TLW	BW	CRW	p-value
C1	109	14.29	5.07	0	35.66	4.98	7.09	0.56
C2	105	14.29	0	0.04	52.06	23.34	25.46	0.31
C3	133	7.69	1.34	0	74.86	5.25	7.34	< 0.01
C4	141	7.14	1.15	0	82.73	3.04	5.13	0.50
C5	102	17.13	3.29	0	45.96	8.75	10.87	0.01
C6	133	8.24	3.13	0	138.23	20.23	22.32	< 0.01
C7	138	8.24	1.12	0	84.34	47.26	49.35	0.42
C8	134	7.14	2.01	0	57.99	5.98	8.07	0.34
C9	129	10.99	1.75	0	67.57	8.82	10.92	0.01
C10	93	26.92	0	1.46	68.97	11.36	13.49	0.01
C11	133	7.14	0.87	0	97.88	51.78	53.87	0.01
C12	131	4.46	0	0.75	83.53	11.49	13.59	< 0.01
C13	142	6.59	1.28	1.41	63.22	0	2.09	< 0.01
C14	140	6.59	0	1.89	68.91	6.85	8.94	< 0.01
C15	122	11.54	1.99	0	29.24	9.08	11.18	0.34
C16	80	24.16	1.75	0	17.03	6.96	9.12	0.21
C17	139	6.04	1.44	0	93.91	53.84	54.11	0.03
C18	90	19.23	4.73	0	51.50	0.25	2.39	0.02
C19	111	13.74	0.59	0	100.26	32.23	34.34	0.04
C20	135	7.73	0.13	0	82.93	13.59	15.69	0.11
C21	114	14.92	1.83	0	69.09	7.56	9.67	0.24
C22	112	14.92	1.42	0	48.51	5.29	7.40	0.30

Table S2.2: Delta AICc results for each individual grizzly bear, where n represents the number of steps in the movement path analyzed (using threshold angle of 10°) and '% missing' is the percentage of locations that were missing in the original movement path. We also present the p-value of the test of absolute fit (based on step length distribution) of the best model.

ID	n	% missing	$CCRW_A$	$CCRW_L$	TLW	BW	CRW	p-value
G1	393	14.66	0	24.33	171.41	183.69	177.47	< 0.01
G2	194	26.57	2.71	0	83.88	64.56	56.27	0.12
G3	315	15.14	0	6.66	71.66	117.56	105.87	0.01
G4	405	16.50	0	36.72	150.94	243.65	242.03	< 0.01
G5	398	11.38	0	32.36	68.69	412.65	405.28	0.03
G6	461	6.08	0	1.55	172.45	203.90	192.49	< 0.01
G7	355	6.93	0	19.92	106.40	187.83	178.43	0.01
G8	350	12.84	0	16.14	40.03	194.93	196.96	< 0.01
G9	437	7.72	21.27	0	281.93	334.10	306.12	0.17
G10	458	4.96	0	5.10	195.37	277.31	261.55	0.01
G11	458	4.45	0	3.93	110.78	187.88	182.06	< 0.01
G12	199	28.98	0	25.72	62.02	190.82	182.45	0.98
G13	159	17.77	0	0.40	24.03	22.95	24.86	0.01
G14	287	20.17	0	1.72	56.61	26.54	23.89	< 0.01
G15	431	6.54	12.80	0	154.32	190.77	188.33	0.01
G16	482	7.32	0	56.63	99.19	583.08	577.94	< 0.01
G17	251	16.20	0	1.81	103.06	199.98	196.90	0.04
G18	140	6.08	0	47.24	80.10	52.21	41.81	< 0.01
G19	289	21.97	13.92	0	159.68	131.01	124.74	0.48
G20	287	23.21	2.91	0	19.97	111.09	112.98	0.05

Table S2.3: Delta AICc results for each individual polar bear, where n represents the number of steps in the movement path analyzed (using threshold angle of 10°) and '% missing' is the percentage of locations that were missing in the original movement path. We also present the p-value of the test of absolute fit of the best model (based on step length distribution).

ID	n	% missing	$CCRW_A$	$CCRW_L$	TLW	BW	CRW	p-value
P1	1,074	25.16	0	8.76	1,398.28	374.81	84.80	< 0.01
P2	1,360	15.77	0	60.14	1,486.26	1,355.13	1,265.14	0.03
P3	1,471	2.41	0	18.54	1,892.33	965.47	448.54	< 0.01
P4	1,469	10.28	0	70.53	1,444.72	574.41	268.71	< 0.01
P5	1,283	17.99	0	9.82	1,616.24	586.28	199.34	< 0.01
P6	108	21.24	2.44	0	116.88	49.68	11.54	0.01
P7	1,692	1.92	0	29.51	1,937.54	851.69	419.61	< 0.01
P8	1,201	18.31	0	11.22	1,422.85	557.77	216.78	< 0.01
P9	1,551	5.53	0	10.66	2,027.95	777.00	270.71	< 0.01
P10	593	26.17	0.76	0	1,014.32	505.28	33.03	< 0.01
P11	1,603	3.61	18.30	0	1,981.57	868.97	307.12	< 0.01
P12	1,178	22.74	0	212.32	710.38	1,167.30	1,042.83	< 0.01

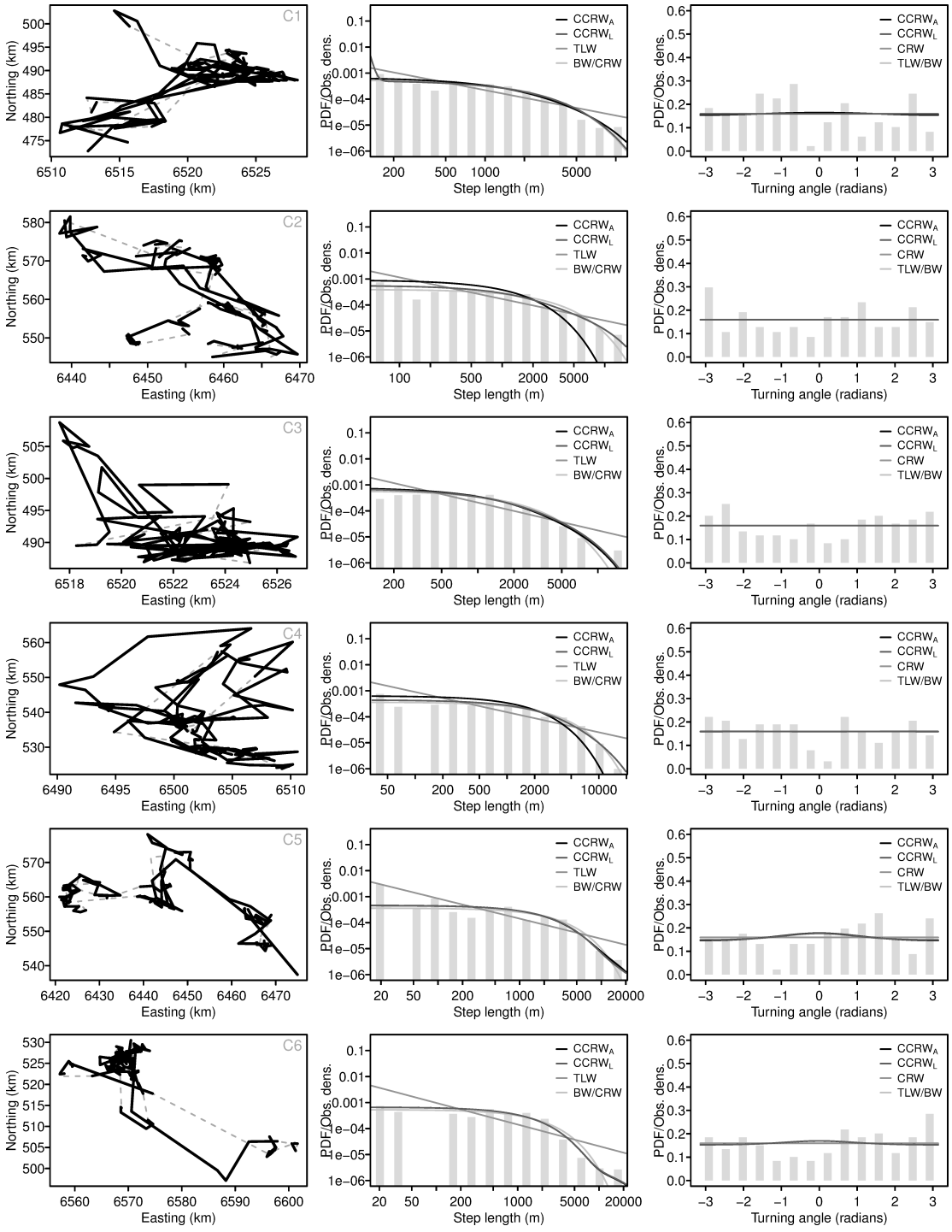

Figure S2.1: Results for each individual caribou. The 1st column shows movement paths (black lines) with missing data identified by grey dashed lines. The 2nd column shows the observed step length frequency and the probability density function (PDF) of models. The 3rd column shows the turning angle frequency and the model PDFs. The figure continues on the next pages.

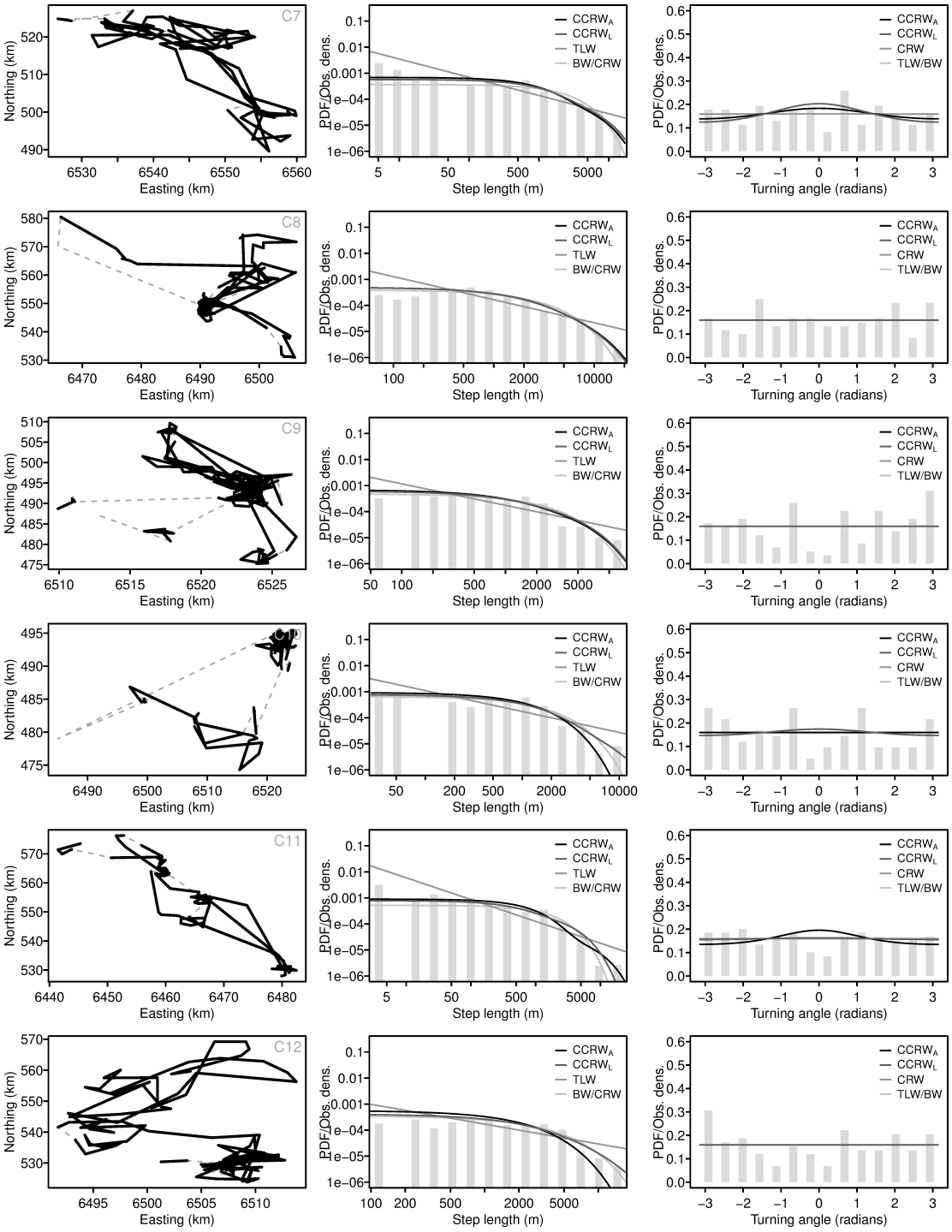

Figure S2.1: Continued

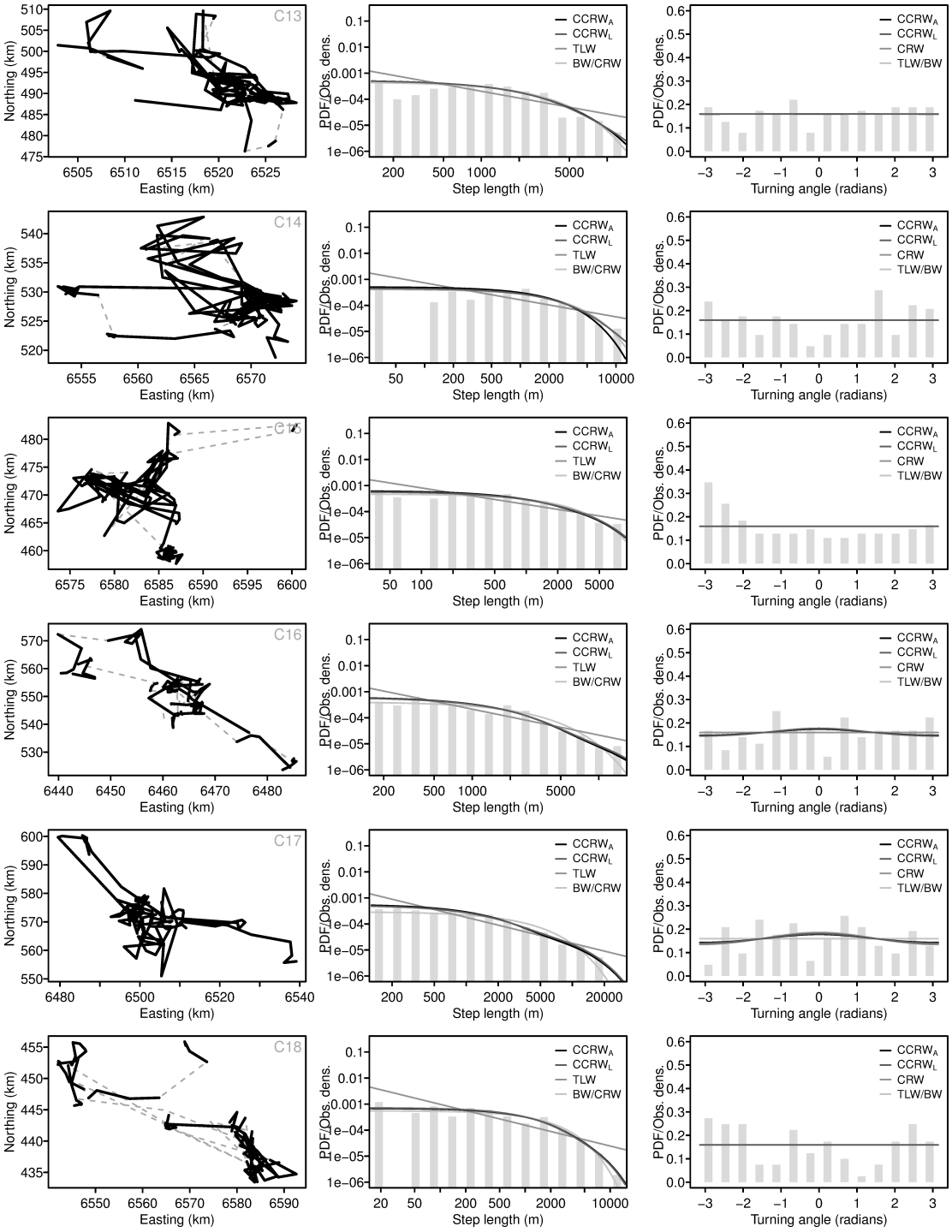

Figure S2.1: Continued

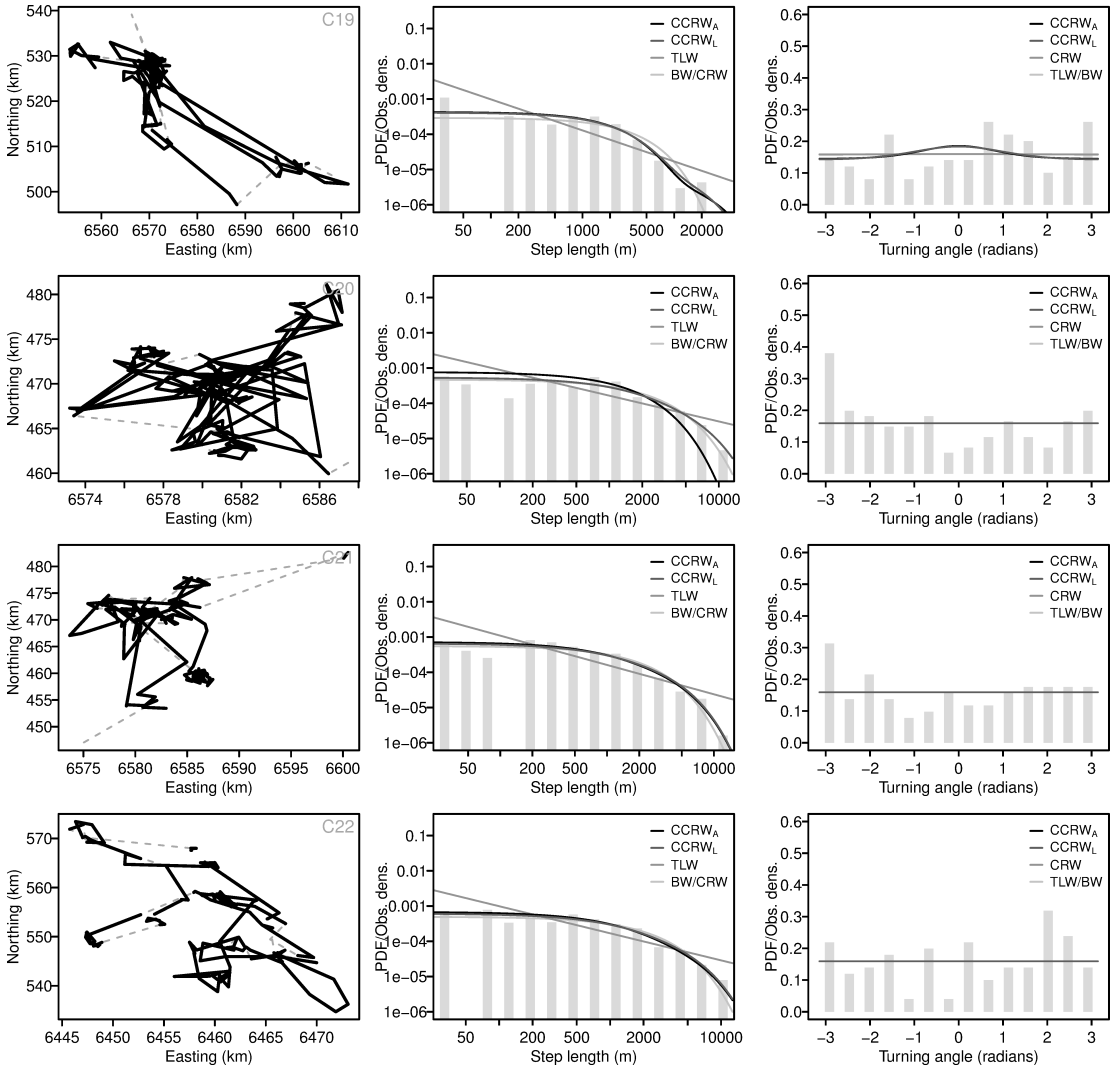

Figure S2.1: Continued

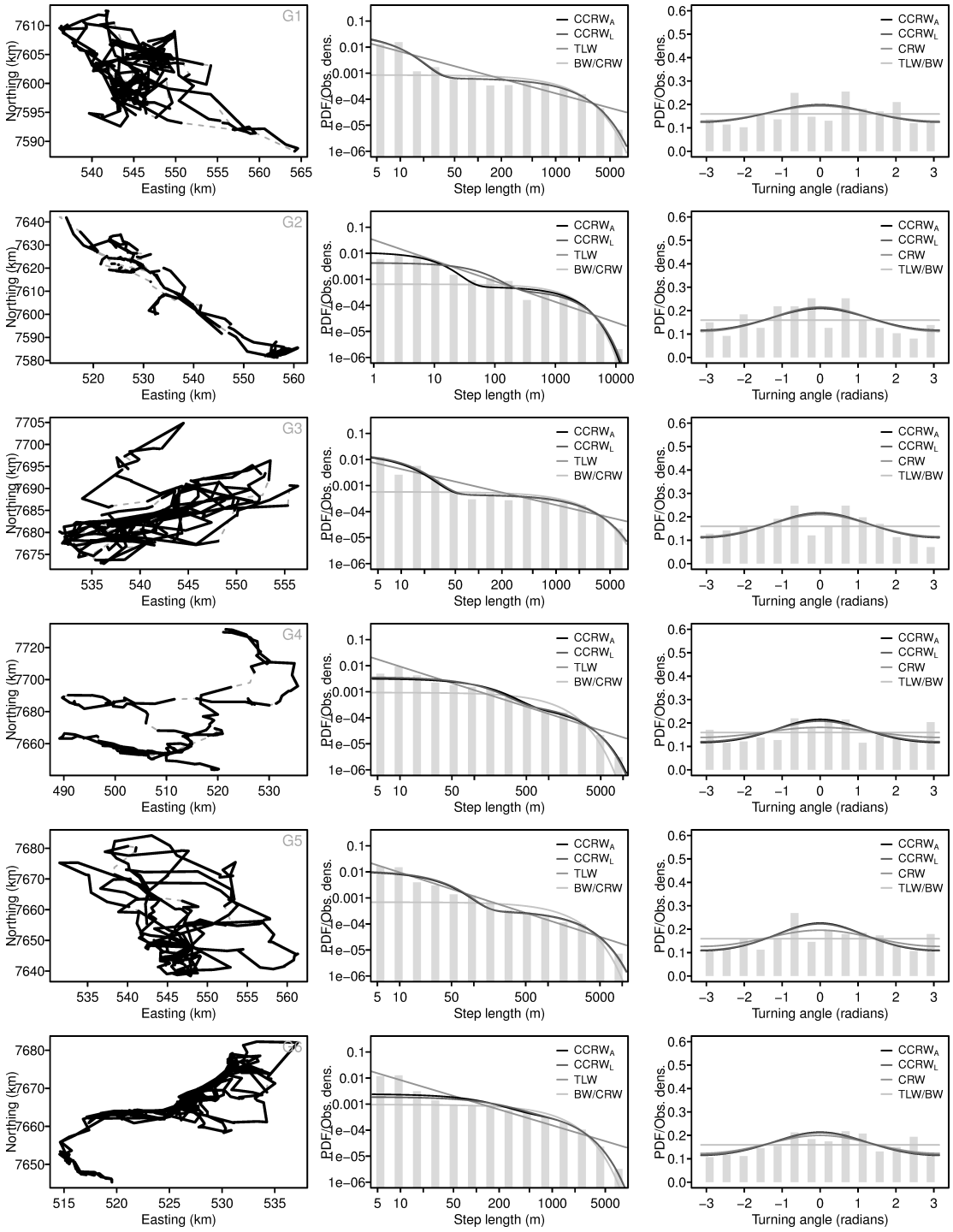

Figure S2.2: Results for each individual grizzly bear. The 1st column shows movement paths (black lines) with missing data identified by grey dashed lines. The 2nd column shows the observed step length frequency and the probability density function (PDF) of models. The 3rd column shows the turning angle frequency and the model PDFs. The figure continues on the next pages.

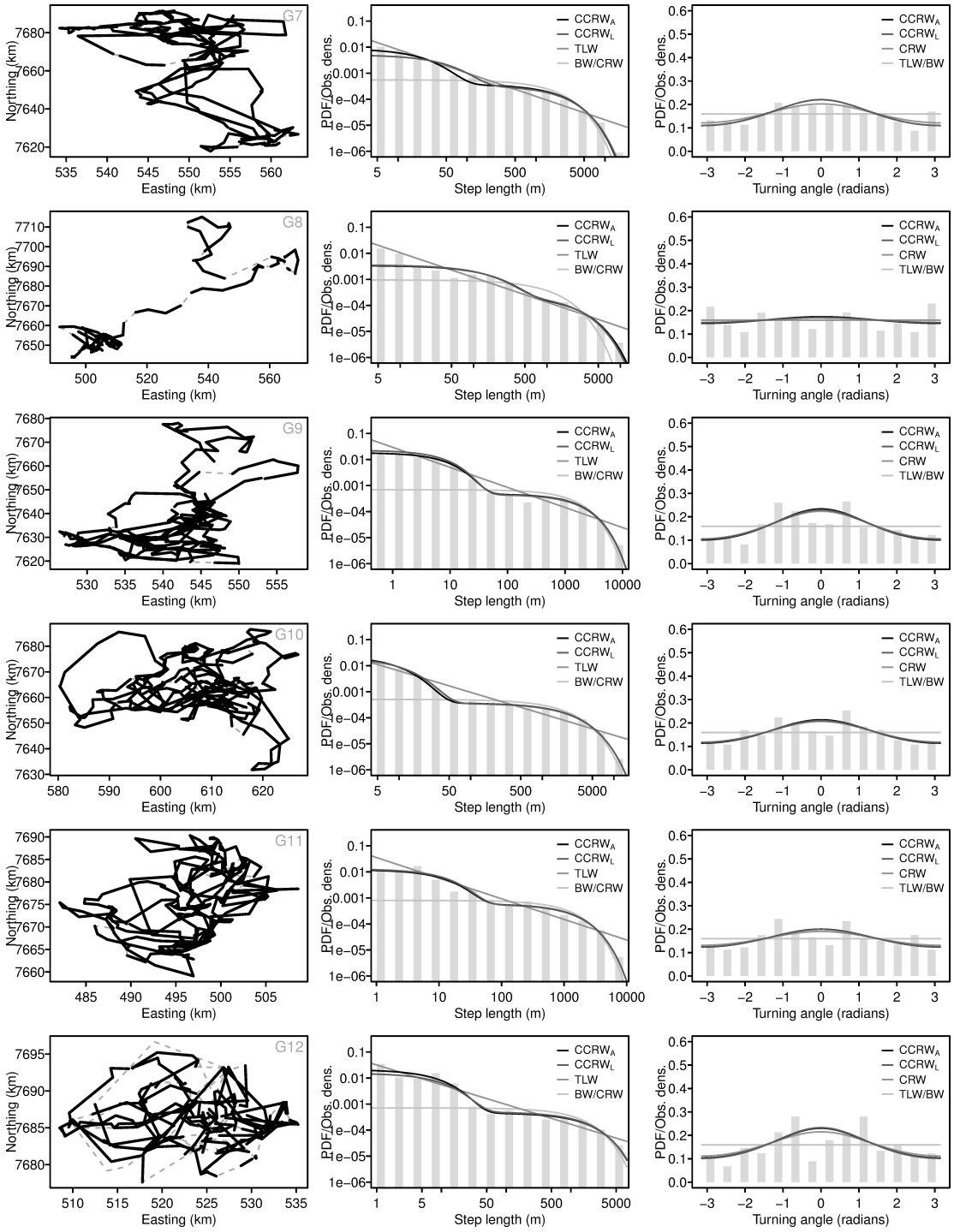

Figure S2.2: Continued

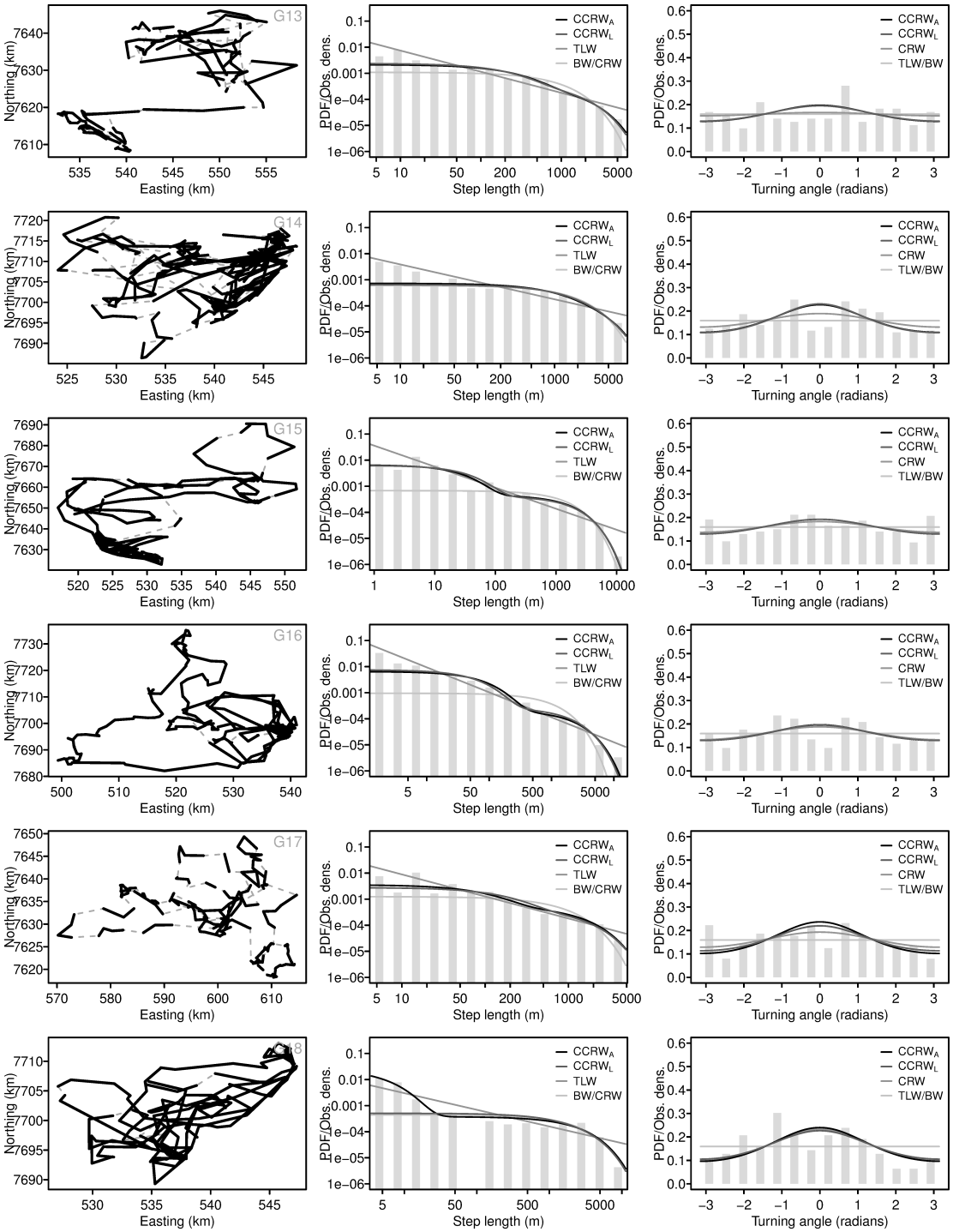

Figure S2.2: Continued

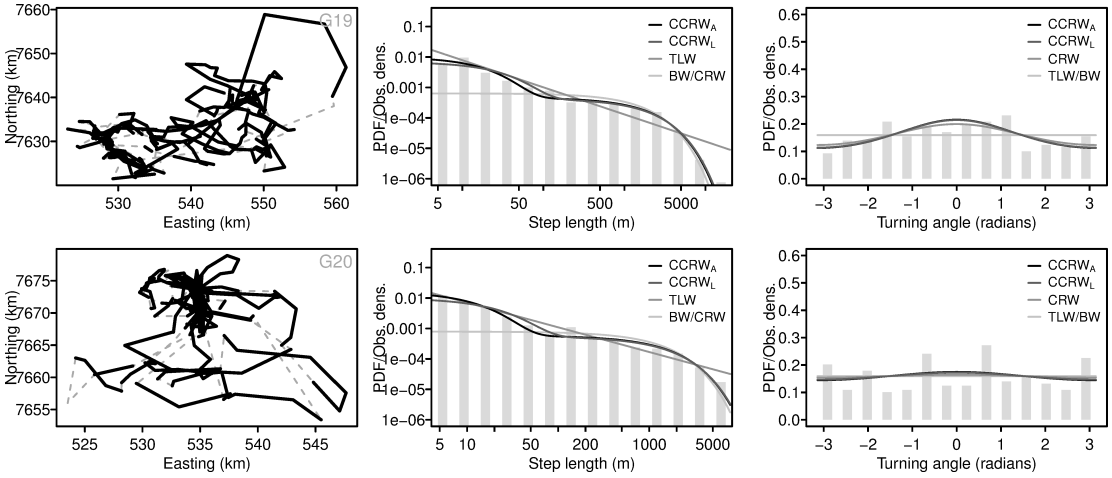

Figure S2.2: Continued

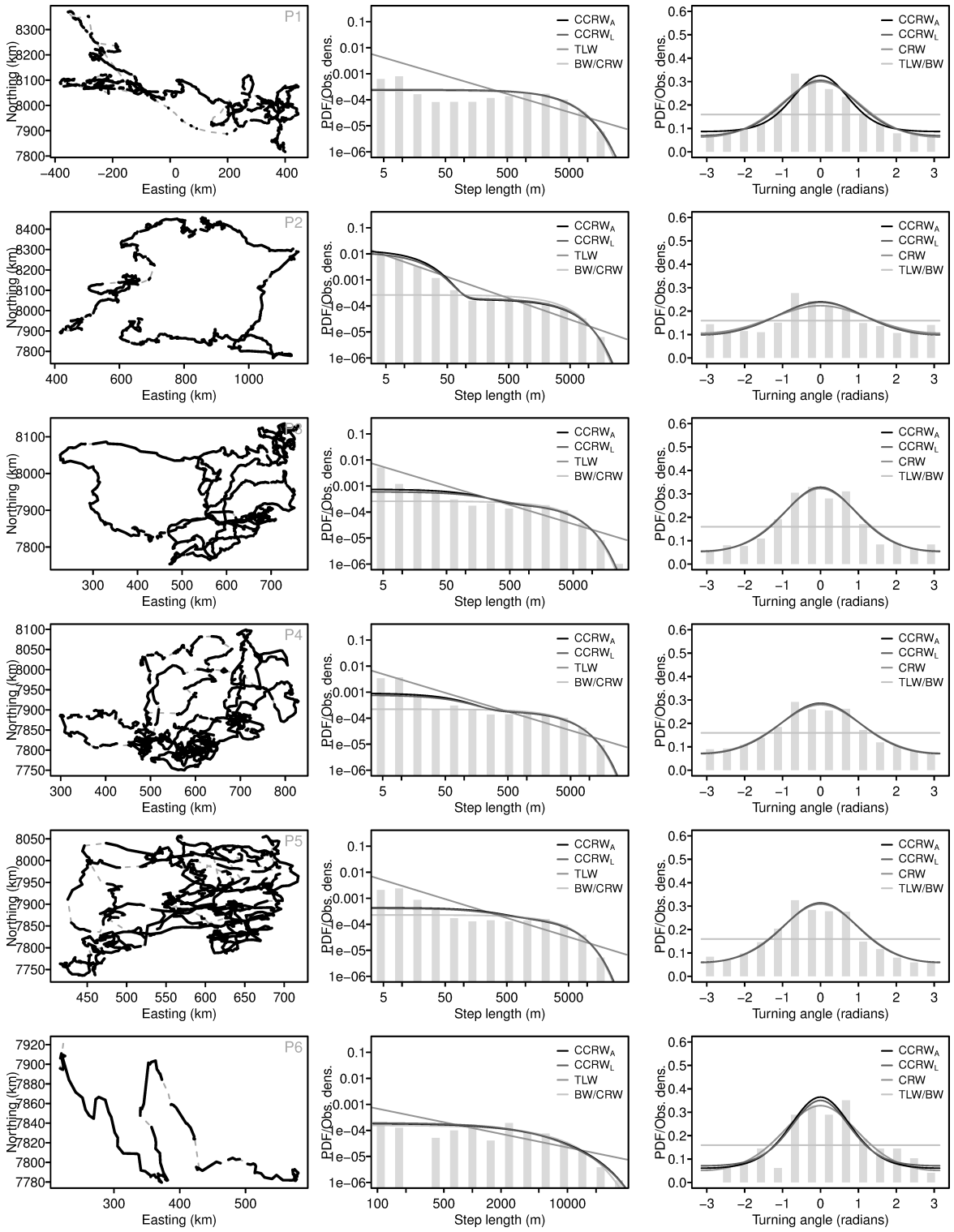

Figure S2.3: Results for each individual polar bear. The 1st column shows movement paths (black lines) with missing data identified by grey dashed lines. The 2nd column shows the observed step length frequency and the probability density function (PDF) of models. The 3rd column shows the turning angle frequency and the model PDFs. The figure continues on the next page.

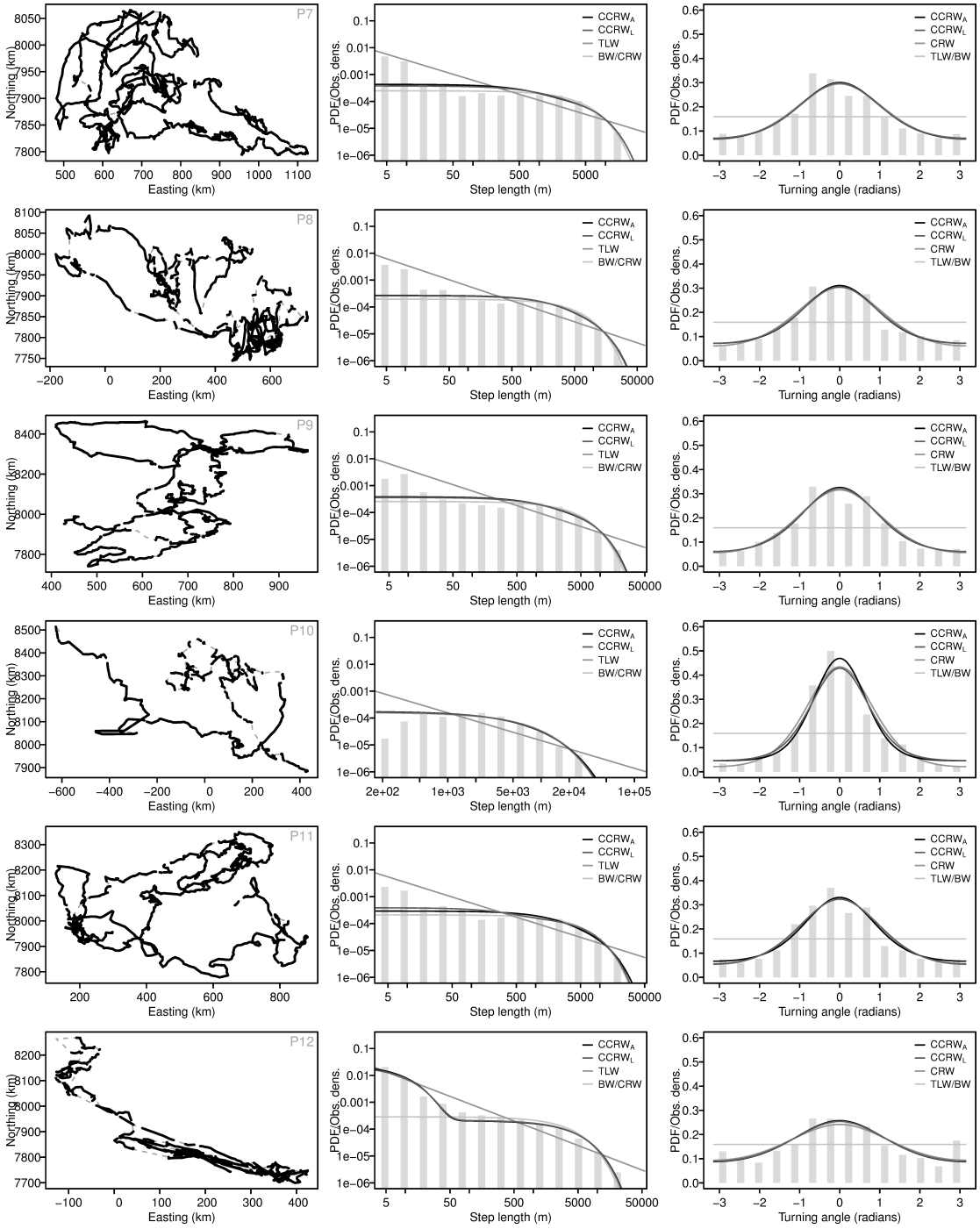

Figure S2.3: Continued

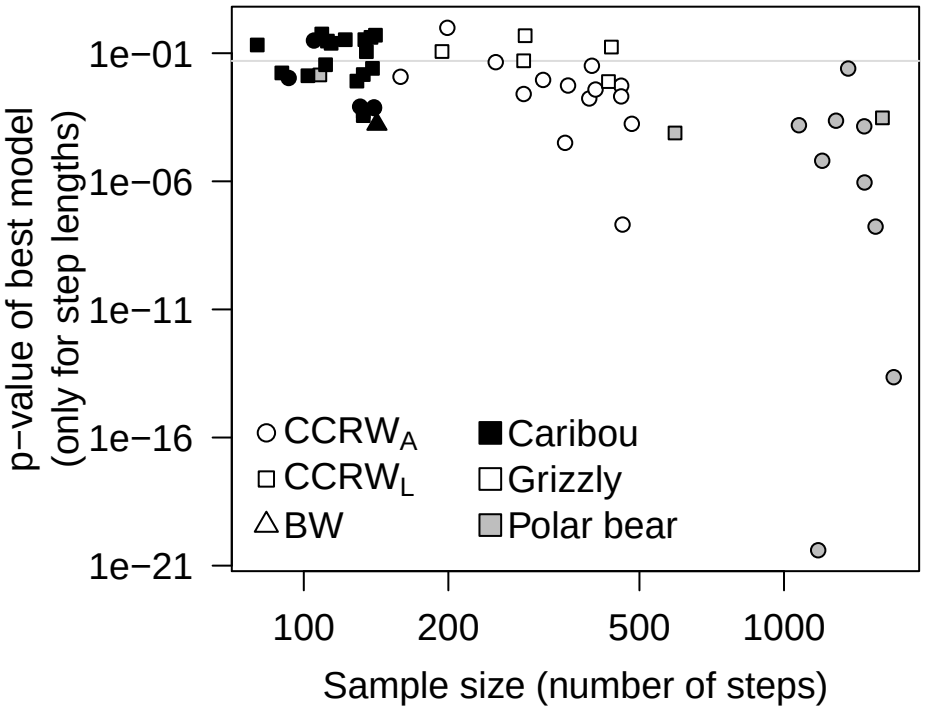

Figure S2.4: Relationship between the absolute fit of the best model and the size of movement paths. The p-values are based solely on step lengths. The color of symbols represents the species, while their shape represents the model selected as best. The grey line indicates the critical value used for the analyses: $\alpha = 0.05$.

S3 Additional CCRW model

As mentioned in Auger-Méthé *et al.* (2015), changing the step length and turning angle distributions could affect the relative and absolute fit of CCRWs. The CCRW only assumes that the movement behaviour can be divided into two phases that differ in their speed and tortuousity, and some authors have used other step length and turning angle distributions to model the CCRW. In particular, the Weibull distribution has been used for step lengths and the wrapped Cauchy distribution has been used for turning angles (Morales *et al.*, 2004; Langrock *et al.*, 2012). Here, we explored whether using the Weibull and wrapped Cauchy changes the fit of CCRWs. Our new model, CCRW_{L_2}, was based on the CCRW_{L} because it is the most flexible version of the CCRW. The only difference is that the new model used the Weibull in place of the exponential distribution and the wrapped Cauchy in place of the von Mises distribution. The likelihood functions of all models and the probability density functions of all distributions are shown in Tables S3.1 and S3.2.

As shown in Table S3.3, the new model, CCRW_{L_2}, was often selected as best model. However, both the CCRW_{A} and CCRW_{L} remained the best models for some individuals, which indicates that the combination of exponential and von Mises distributions was better for some individuals, while the combination of the Weibull and wrapped Cauchy distributions was better for other individuals. Some of the movement paths that were best explained by the new model were not statistically different from it. Considering all three versions did increase the overall number of individuals that were adequately described by a CCRW from 28% (15/54, see main text) to 37% (20/54). It is possible that we could further increase the overall fit of CCRWs by investigating a wider variety of step length and turning angle distributions.

Table S3.1: Likelihood functions and number of parameters to estimate (k) for the six models. For a description of the probability density functions: $\psi_{\mathrm{T}}(l)$, $v_0(\theta)$, $\phi(l)$, $v(\theta)$, $w(l)$, and $c(\theta)$, see Table S3.2.

Model	Likelihood function	k
TLW	$\prod_{t=1}^{n}\ \psi_{\mathrm{T}}(l_t\|\mu_{\mathrm{T}},a,b)\ v_0(\theta_t)$	3
BW	$\prod_{t=1}^{n}\ \phi(l_t\|\lambda,a)\ v_0(\theta_t)$	3
CRW	$\prod_{t=1}^{n}\ \phi(l_t\|\lambda,a)\ v(\theta_t\|\kappa)$	4
$\mathrm{CCRW_A}$	$\prod_{t=1}^{n}\boldsymbol{\Gamma}_t\begin{pmatrix}\phi(l_t\|\lambda_{\mathrm{I}},a)\,v_0(\theta_t) & 0\\ 0 & \phi(l_t\|\lambda_{\mathrm{E}},a)\,v(\theta_t\|\kappa_{\mathrm{E}})\end{pmatrix}\begin{pmatrix}1\\1\end{pmatrix}$, $\boldsymbol{\Gamma}_t=\begin{cases}\begin{pmatrix}\delta_{\mathrm{I}} & 1-\delta_{\mathrm{I}}\end{pmatrix} & \text{if } t=1\\ \begin{pmatrix}\gamma_{\mathrm{II}} & 1-\gamma_{\mathrm{II}}\\ 1-\gamma_{\mathrm{EE}} & \gamma_{\mathrm{EE}}\end{pmatrix} & \text{otherwise}\end{cases}$	7
$\mathrm{CCRW_L}$	$\prod_{t=1}^{n}\boldsymbol{\Gamma}_t\begin{pmatrix}\phi(l_t\|\lambda_{\mathrm{I}},a)\,v_0(\theta_t) & 0\\ 0 & \phi(l_t\|\lambda_{\mathrm{E}},a)\,v(\theta_t\|\kappa_{\mathrm{E}})\end{pmatrix}\begin{pmatrix}1\\1\end{pmatrix}$, $\boldsymbol{\Gamma}_t=\begin{cases}\boldsymbol{\delta}\ ^{\dagger} & \text{if } t=1\\ \begin{pmatrix}0 & 1-\gamma_{\mathrm{I}}(1) & \dots & 0 & \gamma_{\mathrm{I}}(1) & \dots & 0\\ \vdots & \ddots & \ddots & \vdots & \vdots & \dots & \vdots\\ 0 & 0 & \dots & 1-\gamma_{\mathrm{I}}(m-1) & \gamma_{\mathrm{I}}(m-1) & \dots & 0\\ 0 & 0 & \dots & 1-\gamma_{\mathrm{I}}(m) & \gamma_{\mathrm{I}}(m) & \dots & 0\\ \gamma_{\mathrm{E}}(1) & 0 & \dots & 0 & 1-\gamma_{\mathrm{E}}(1) & \dots & 0\\ \vdots & \vdots & \dots & \ddots & \ddots & \ddots & \vdots\\ \gamma_{\mathrm{E}}(m-1) & 0 & \dots & 0 & 0 & \dots & 1-\gamma_{\mathrm{E}}(m-1)\\ \gamma_{\mathrm{E}}(m) & 0 & \dots & 0 & 0 & \dots & 1-\gamma_{\mathrm{E}}(m)\end{pmatrix}^{\ddagger} & \text{otherwise}\end{cases}$	6
$\mathrm{CCRW_{L_2}}$	$\prod_{t=1}^{n}\boldsymbol{\Gamma}_t\begin{pmatrix}w(l_t\|\beta_{\mathrm{I}},\eta_{\mathrm{I}})\,v_0(\theta_t) & 0\\ 0 & w(l_t\|\beta_{\mathrm{E}},\eta_{\mathrm{E}})\,c(\theta_t\|\rho_{\mathrm{E}})\end{pmatrix}\begin{pmatrix}1\\1\end{pmatrix}$, $\boldsymbol{\Gamma}_t=\begin{cases}\boldsymbol{\delta}\ ^{\dagger} & \text{if } t=1\\ \begin{pmatrix}0 & 1-\gamma_{\mathrm{I}}(1) & \dots & 0 & \gamma_{\mathrm{I}}(1) & \dots & 0\\ \vdots & \ddots & \ddots & \vdots & \vdots & \dots & \vdots\\ 0 & 0 & \dots & 1-\gamma_{\mathrm{I}}(m-1) & \gamma_{\mathrm{I}}(m-1) & \dots & 0\\ 0 & 0 & \dots & 1-\gamma_{\mathrm{I}}(m) & \gamma_{\mathrm{I}}(m) & \dots & 0\\ \gamma_{\mathrm{E}}(1) & 0 & \dots & 0 & 1-\gamma_{\mathrm{E}}(1) & \dots & 0\\ \vdots & \vdots & \dots & \ddots & \ddots & \ddots & \vdots\\ \gamma_{\mathrm{E}}(m-1) & 0 & \dots & 0 & 0 & \dots & 1-\gamma_{\mathrm{E}}(m-1)\\ \gamma_{\mathrm{E}}(m) & 0 & \dots & 0 & 0 & \dots & 1-\gamma_{\mathrm{E}}(m)\end{pmatrix}^{\ddagger} & \text{otherwise}\end{cases}$	7

† As in Langrock *et al.* (2012), we are using the stationary distribution for the initial values, $\boldsymbol{\delta}$, of the Markov chain for $\mathrm{CCRW_L}$.

‡ As in Langrock *et al.* (2012), $\gamma_{\mathrm{I}}(r)=\frac{p_{\mathrm{I}}(r)}{\left(1-\sum_{k=1}^{r-1}p_{\mathrm{I}}(r)\right)}$ and $\gamma_{\mathrm{E}}(r)=\frac{p_{\mathrm{E}}(r)}{\left(1-\sum_{k=1}^{r-1}p_{\mathrm{E}}(r)\right)}$. For both phases, we are using a Poisson distribution, $p_{\mathrm{I}}(r)$ and $p_{\mathrm{E}}(r)$, for the state dwell time. See Table S3.2 for a description of the Poisson distribution $p(r)$.

Table S3.2: Formulas for the probability density functions (PDFs) used in the models and the restrictions on their variables and parameters. The variables l and θ represent step length and turning angle, respectively.

Distribution	Symbol	PDF	Restrictions
Exponential	$\phi(l\|\lambda, a)$	$\lambda\, e^{-\lambda(l-a)}$	$a \leq l, \quad \lambda > 0$
Weibull	$w(l\|\beta, \eta)$	$\left(\frac{\beta l^{\beta-1}}{\eta^{\beta}}\right) e^{-\left(\frac{l}{\eta}\right)^{\beta}}$	$\beta > 0, \eta > 0$
Truncated Pareto	$\psi_{\mathrm{T}}(l\|\mu_{\mathrm{T}}, a, b)$	$\frac{(\mu_{\mathrm{T}}-1)\, l^{-\mu_{\mathrm{T}}}}{a^{1-\mu_{\mathrm{T}}}-b^{1-\mu_{\mathrm{T}}}}$	$a \leq l \leq b$ †
Von Mises	$v(\theta\|\kappa)$	$\frac{1}{\int_{-\pi}^{\pi} e^{\kappa\cos(\theta)} d\theta} e^{\kappa\cos(\theta)}$ ‡,§	$\kappa > 0$
Uniform	$v_0(\theta)$	$\frac{1}{2\pi}$	
Wrapped Cauchy	$c(\theta\|\rho)$	$\frac{1}{2\pi}\left(\frac{1-\rho^2}{1+\rho^2-2\rho\cos(\theta)}\right)$ §	$0 < \rho < 1$
Poisson	$p(r\|\alpha)$	$\frac{\alpha^r}{r!} e^{-\alpha}$	$\alpha > 0$

† Unlike in Auger-Méthé *et al.* (2015), we are not placing restrictions on the estimated μ_{T} values.

‡ This is a simplified and expanded equation of the von Mises PDF. The same equation is often written with a modified Bessel function of the first kind and of order 0.

§ These simplified versions assume that the distribution is centred at 0, for full version see Codling, Plank & Benhamou (2008).

Table S3.3: Relative and absolute fit of the six models on the movement paths of 22 caribou, 20 grizzlies, and 12 polar bears. For each model, we present the number of movement paths selected as best model with AIC_c and the mean Akaike weight, w, of these selected paths. We also present how many of the selected paths are not different from this model according to a test of absolute fit based on the step length distribution.

Model	N° as best model			w of best model			N° p-value > 0.05		
	Caribou	Grizzly	Polar bear	Caribou	Grizzly	Polar bear	Caribou	Grizzly	Polar bear
$CCRW_A$	1	8	3	0.47	0.89	1	1	1	0
$CCRW_L$	8	3	2	0.53	0.86	0.64	5	3	0
$CCRW_{L_2}$	13	9	7	0.85	0.87	1	7	3	0
TLW	0	0	0	–	–	–	–	–	–
BW	0	0	0	–	–	–	–	–	–
CRW	0	0	0	–	–	–	–	–	–

Literature Cited

Auger-Méthé, M., Derocher, A.E., Plank, M.J., Codling, E.A. & Lewis, M.A. (2015) Differentiating the Lévy from a composite correlation random walk. *Methods in Ecology and Evolution*, **6**, 1179–1189.

Codling, E.A. & Plank, M.J. (2011) Turn designation, sampling rate and the misidentification of power laws in movement path data using maximum likelihood estimates. *Theoretical Ecology*, **4**, 397–406.

Codling, E.A., Plank, M.J. & Benhamou, S. (2008) Random walk models in biology. *Journal of the Royal Society Interface*, **5**, 813–834.

Langrock, R., King, R., Matthiopoulos, J., Thomas, L., Fortin, D. & Morales, J.M. (2012) Flexible and practical modeling of animal telemetry data: hidden Markov models and extensions. *Ecology*, **93**, 2336–2342.

Morales, J.M., Haydon, D.T., Frair, J., Holsinger, K.E. & Fryxell, J.M. (2004) Extracting more out of relocation data: building movement models as mixtures of random walks. *Ecology*, **85**, 2436–2445.

Reynolds, A.M., Smith, A.D., Menzel, R., Greggers, U., Reynolds, D.R. & Riley, J.R. (2007) Displaced honey bees perform optimal scale-free search flights. *Ecology*, **88**, 1955–1961.